European Journal of Mechanics B/Fluids 28 (2009) 136–145

Contents lists available at ScienceDirect

European Journal of Mechanics B/Fluids

www.elsevier.com/locate/ejmflu

Numerical experiments on the transient motions of a flapping foil

Laura Guglielmini [a,*], Paolo Blondeaux [b]

[a] Department of Engineering and Applied Sciences, Harvard University 29 Oxford Street, Cambridge, MA 02138, USA
[b] Department of Civil, Environmental and Architectural Engineering, University of Genova, Via Montallegro 1, 16145 Genova, Italy

ARTICLE INFO

Article history:
Received 10 July 2007
Received in revised form 29 May 2008
Accepted 29 May 2008
Available online 4 June 2008

Keywords:
Fish swimming
Flapping foils
Fast-start manoeuvre

ABSTRACT

The flow field generated by a foil during transient motions is investigated by means of numerical experiments. The numerical simulations have some advantages with respect to laboratory experiments. Indeed, having access to the velocity and pressure fields both in space and in time, it is possible to 'measure' quantities like vorticity, forces and torques which are quite difficult to obtain in laboratory. Moreover, data can be easily gained for different foil kinematics. The obtained results show that the time history of the propulsive force strongly depends on the details of the kinematics of the foil. Moreover, the numerical simulations have allowed to understand the main mechanisms employed by fish to propel themselves during fast starts and to identify the values of the parameters providing optimal propulsive performances.

1. Introduction

In the last decades a new research field has been initiated, named 'bionics', which includes the study of the principles of flapping fin propulsion. An analysis of the performances of fish show that fish possess some hydrodynamic properties which are superior to those of actual underwater vehicles propelled by rotating thrusters. Therefore, the dynamics of flapping fins is currently investigated to exploit their use on small water vehicles for operations in different extreme conditions. The interest in propulsive flapping fin devices is also justified by the observation that propulsive systems with flapping foils (i) combine the function of propulsor, control device and stabilizer thus providing a high maneuverability, (ii) possess a sufficiently high efficiency, (iii) have relatively low aerodynamic drag in the 'switched-off' position, (iv) are relatively low-frequency systems and, hence, generate less mechanical problems, (v) can operate efficiently in different regimes of motion.

The fin/foil motions can be classified into two broad categories on the basis of the their temporal features: (a) periodic (steady) motions, characterized by a cyclic repetition of the propulsive movements; (b) transient (unsteady) motions. Periodic motions are employed to propel a vehicle for relatively large distances at a more or less constant speed, while transient motions include those required for manoeuvres like starts, stops, turns,....

A large number of the available investigations are devoted to the study of the steady motions. Using two-dimensional numerical simulations [11,12,14,15] studied the dynamics of oscillating foils and identified the values of the parameters giving rise to optimal propulsive performances. In the two-dimensional approximation, only the cross-stream component of the vorticity is taken into account. Therefore, the propulsive efficiency is overestimated due to the underestimation of the wake energy loss. However, the first three-dimensional simulations of [4] and [7] seem to support the main finding of the two-dimensional approaches at least when the span of the foil is large enough.

On the other hand, there are relatively few studies of the unsteady motions of flapping fins. Attention has been mainly focused on manoeuvring fish and flow visualization studies have shown the important role of the shedding and control of vorticity by the moving fins in the generation of the propulsive force. Indeed, manoeuvring by fish usually involves the coordinate use of median, paired and caudal fins as well as the use of body bending which generate a complex vorticity field.

Even though the whole body of the fish contributes to provide the acceleration which is necessary during rapid manoeuvres, an essential role in the manoeuvres is played by the fish tail. By analyzing the kinematics of the tail, described a.o. by [5,16] and reproduced by [6], it can be argued that during fast starts the tail bends sideways to an angle α and simultaneously starts to move in the transverse direction. After having reached the maximum lateral displacement, an opposite rotation is performed and the tail starts a new movement in the transverse direction returning to its original position.

Ahlborn et al. [2] proposed a simple model to simulate the kinematics of the tail of a fish which performs a fast start. Indeed, the tail is supposed to be approximated by a plate which rotates around its leading edge up to a maximum value α_{max} and then returns to its original position. In their laboratory ex-

* Corresponding author.
E-mail addresses: laurag@deas.harvard.edu (L. Guglielmini), paolo.blondeaux@unige.it (P. Blondeaux).

0997-7546/$ – see front matter
doi:10.1016/j.euromechflu.2008.05.005

periments, they determined the dynamics of the vortex structures shed by the rotating plate by means of flow visualizations and measured the propulsive force. Moreover, they proposed a vortex production-destruction model which suggests a quantitative difference in the thrust production of the initial sideways flip and of the return stroke. Although kinematically identical, according to [2], the first flip would essentially set up a vortex and thereby exert a sideways reaction force onto the fish while the return stroke would essentially stop the rotational motion of the vortex and produce forward thrust. Measurements of the thrust and the impulse produced by the tail model reveal distinctive phases of motion relevant to the fast-start: (i) a negative precursor, (ii) an impulse-generating phase in which the sideways flow is deflected towards the rear, (iii) a maximum thrust phase where the direction of momentum is inverted. Phases (i) and (iii) produce an active wake with vortices that turn in the opposite sense to the von Karman street vortices in the wake of a dragged object.

In the present work fast starts, which can be seen as a prototype of rapid manoeuvres, are investigated by means of numerical simulations. Even though three-dimensional flow data start to be collected in laboratory by means of the PIV measuring technique [13], and the projections of the flow onto different planes allow a reconstruction of the three-dimensional flow, numerical experiments have some advantages with respect to laboratory experiments. Indeed, having access to the velocity and pressure fields both in space and in time, it is possible to 'measure' quantities like vorticity, strain, dissipation etc., which are quite difficult to obtain in laboratory. Moreover, also the forces acting on the foil can be easily computed.

As in Ahlborn et al. [2], the flow is supposed to be two-dimensional and the problem is written in the vorticity-stream function formulation. Readers familiar with aerodynamics wing theory will recognize that a two-dimensional approach overestimates efficiency because it takes into account only the energy of cross-stream wake vorticity (at right angle to the direction of motion) although in reality trailing vorticity (parallel to the direction of motion) might also be present. However, a two-dimensional approach can provide useful information on the dynamics of the large scale vortical structures shed by the foil and on the forces acting on it [15]. Moreover, it is known that three-dimensional effects become negligible when the ratio between the span and the chord of the oscillating foil is larger than four [8]. This fact has been recently confirmed by the three-dimensional numerical simulations of the flow generated by a foil of finite span made by Blondeaux et al. [4] and Dong et al. [7]. Indeed the vorticity field computed by [4] in the middle plane of a three dimensional foil, characterized by a span equal to three times the chord, is practically coincident with that provided by a two-dimensional approach (see 8 and 9 of [4]). Moreover, [7] have shown that the propulsive efficiency of a foil of aspect-ratio 4 is very close to that of a two-dimensional foil (Figs. 22 and 23 of [7]).

The equations are solved by means of a numerical approach which employs finite difference approximations and spectral methods. Different kinematics of the fish tail are simulated and different indicators of the efficiency of the manoeuvres are evaluated.

2. Formulation of the problem

We consider a two-dimensional foil which mimics a fish tail during a transient motion. In the reference frame (x^*, y^*) moving with the forward velocity $U_0^*(t^*)$ of the foil, the kinematics of the foil, which oscillates in the transverse direction and simultaneously rotates, can be described by providing the vertical coordinate $h_0^*(t^*)$ of the point O around which the foil pitches and the angle $\alpha(t^*)$ (positive in the clockwise direction) which the foil chord forms with the x^*-axis which is supposed to be aligned with the

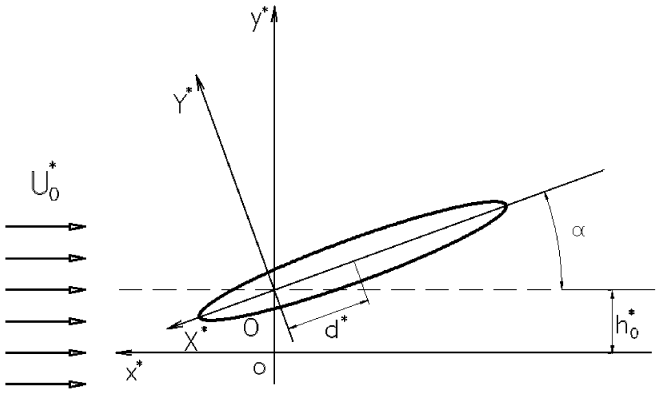

Fig. 1. Inertial reference frame (x^*, y^*) moving with the forward velocity U_0^* and reference frame (X^*, Y^*) moving with the foil.

velocity $U_0^*(t^*)$ (see Fig. 1). The distance of the point O from the center of the chord of the foil is denoted with d^*. The functions describing the kinematics of the tail along with the other parameters of the problem are given later on, while discussing the results. The governing equations, which describe the fluid motion induced by the movements of the foil and provide the forces acting on the foil, are the vorticity equation and the Poisson equation. The vorticity and velocity fields as well as the forces acting on the foil are determined numerically following a procedure which makes use of a spectral method and finite difference approximations. To facilitate the numerical computations, the problem is first written in the non-inertial reference frame (X^*, Y^*) which moves with the foil. Moreover, to simplify the forcing of the no slip condition along the foil surface, we introduce first a conformal mapping such that the section of the foil is transformed in a circle and then a polar coordinate system (r^*, θ). The pressure, which is required to determine the force and the torque acting on the foil, is not calculated explicitly in the vorticity-stream function formulation and it is obtained by means of the momentum equation integrated along the foil surface. We omit, for the sake of brevity, the description of the numerical procedure, which is that employed by [10,11]. The interested reader can find the details of the numerical approach and a description of the tests made to ascertain the reliability and accuracy of the numerical code in the above papers. The results described in the following have been obtained using different numbers N_r and N_θ of grid points in the r- and θ-directions respectively and different values of the time step Δt^*. Moreover, different sizes of the computational box have been used. The standard runs have been made with $N_r = 650$, $N_\theta = 1024$ and a radius of the computational box equal to 5 foil chords. The reader should take into account that the radial coordinate has been stretched to cluster the grid points close to the foil surface where the velocity gradients are higher. Finally, the time step Δt^* has been fixed equal to 10^{-4} the duration of the manoeuvre. Then, to ascertain that the results do not depend on the values of N_r, N_θ and Δt, some of the runs have been repeated doubling the number of points and halving the time step. Moreover, by repeating some of the runs using a radius of computational box equal to 9 chords, it has been checked that the results do not depend on the size of the numerical domain.

3. Validation of the model

As already pointed out, the numerical code used in the present investigation was validated by comparing the numerical results with the experimental data of [3], who measured the velocity field generated by an oscillating foil by using the Particle Image Velocimetry (P.I.V.). This comparison, described in Guglielmini and

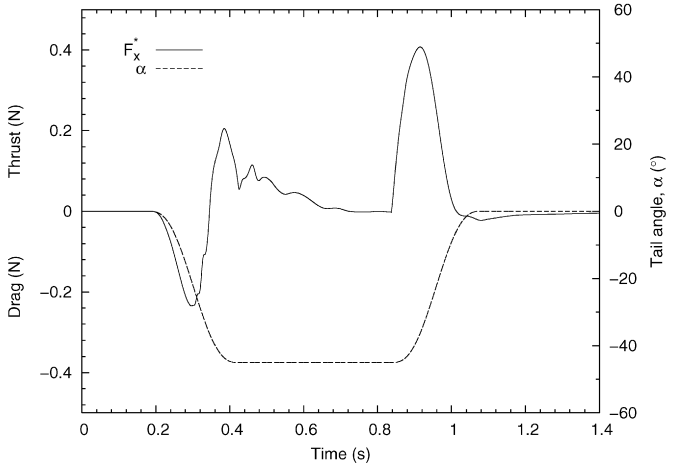

Fig. 2. Horizontal force F_x^* (continuous line) acting on the foil during its excursion with angle $\alpha(t)$ (broken line). Results of a numerical simulation carried out for values of the parameters similar to those of the experiment of [2]. The results are dimensional and can be compared with [2]'s Fig. 4, reproduced in Fig. 3.

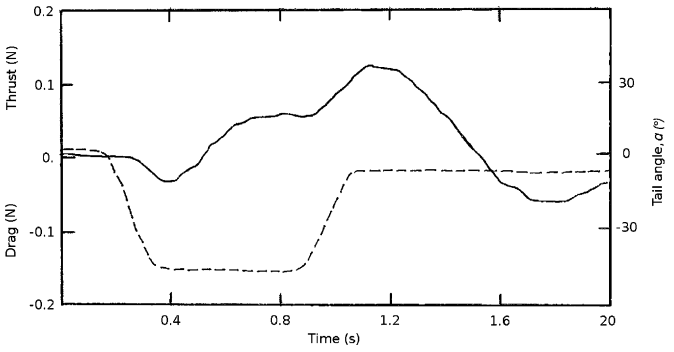

Fig. 3. Horizontal force F_x^* (continuous line) acting on the foil during its excursion with angle $\alpha(t)$ (broken line). Sketch of the experimental results as they appear in Fig. 4 of [2].

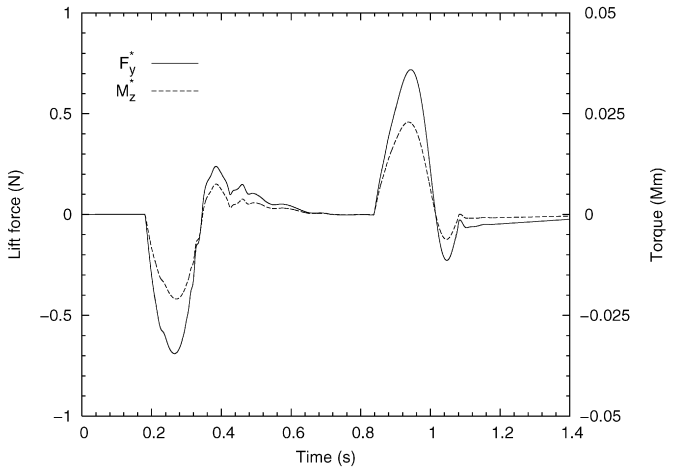

Fig. 4. Vertical force F_y^* and torque M_z^* acting on the foil during its rotation. The parameters are those of the experiment of [2]. The results are dimensional.

Blondeaux [11], shows that the code can reproduce the dynamics of the vortex structures shed by the foil both qualitatively and quantitatively. Moreover the code appears to provide an accurate estimate of the forces acting on the foil.

To provide further support to the reliability of the code and to investigate its performances in the simulation of the flow generated by an aperiodic motion of the foil, an attempt to reproduce the laboratory experiments of Ahlborn et al. [1] is made. In the experiments, a rectangular foil of submerged height equal to 15 cm and chord c^* equal to 5 cm simulates a fish tail. The foil rotates around its leading edge and it does not exhibit any heaving motion. Therefore, we force $h_0^*(t^*)$ to vanish and we fix $d^* = c^*/2$. Finally, the value of α is provided by

$$\alpha(t^*) = \begin{cases} 0 & \text{for } t^* < 0 \\ f_1(t^*) & \text{for } 0 < t^* < T_r^* \\ \alpha_{\max} & \text{for } T_r^* < t^* < T_r^* + T_e^* \\ f_2(t^*) & \text{for } T_r^* + T_e^* < t^* < T^* \\ 0 & \text{for } t^* > T^* \end{cases} \tag{1}$$

where T_r^* is the duration of both the counter-clockwise and clockwise rotations, T_e^* is the time spent by the foil at its maximum rotation and $T^* = 2T_r^* + T_e^*$ is the total duration of the manoeuvre. The functions f_1 and f_2 are fifth order polynomial functions chosen by forcing $\alpha(t^*)$ and its first and second derivatives to be continuous at $t^* = 0, T_r^*$ and at $t^* = T_r^* + T_e^*, T^*$. Notwithstanding the main parameters of the laboratory experiments are reproduced in the numerical experiments, discrepancies between the experimental measurements and the numerical results are expected to be present. Indeed, even though [1] introduced some tricks to limit three-dimensional effects in the experimental apparatus, it is unavoidable that the finite span of the foil used in the laboratory experiments and its interaction with the free surface and the bottom of the tank induced parasitic vorticity components which cause a significant decrease of the propulsive force and hence a damping of the force peaks with respect to the numerical model, which is strictly two-dimensional. In the two-dimensional approximation, the two counter-rotating vortices shed by the trailing edge during its counter-clockwise and clockwise motions keep separate. On the contrary the flow visualizations of [9], who visualized the vortex structures shed by a foil of finite span which is rotated around its leading edge up to an angle of 30° in 0.25 s and then rotated back to 0° at $t = 0.5$ s while moving with a constant forward velocity, show that the vortex structures shed by the trailing edge during its upward and downward motions give rise to a unique vortex ring, being connected by the vorticity shed by the foil tips. Moreover, further quantitative differences between the experimental and numerical results might be introduced by the different geometry of the section of the experimental and numerical foils. In particular, the possible different shape of the trailing edge might induce a different spatial distributions of the vorticity shed by the foil and hence a different dynamics of the vortex structures in the wake of the rotating foil. Finally, even though the rotation (1) of the foil in the numerical simulations is chosen to follow the gross features of the data given by [1] (see Fig. 4 of [1]), it is unavoidable that differences are present between the kinematics of the foil in laboratory and in numerical experiments, in particular if the angular velocities and accelerations are considered. Indeed, [1] do not provide the function $\alpha(t^*)$ (see Eq. (1)) but only a sketch of its time development, so that, while the values of $\alpha(t^*)$ can be reasonably estimated, the correct evaluation of $d\alpha/dt^*$ and $d^2\alpha/dt^{*2}$ is much more difficult.

Therefore, if Fig. 2, where the thrust force obtained by the numerical code is plotted versus time for $\alpha_{\max} = -45°$, $T_r^* = 0.18$ s, $T_e^* = 0.55$ s, $T^* = 0.91$ s, is compared with Fig. 4 of [1] (see also the sketch drawn in Fig. 3), differences are present, even though the gross features of the phenomenon are reproduced. In fact, both the numerical simulation and the experimental measurements reveal the distinct phases already described in the introduction: a negative precursor as the tail rotates counter-clockwise, a gradually increasing thrust, a spike as the tail returns towards its rest position and a gradual decay of the thrust to zero after the tail motion is stopped. However, for the reasons previously described, the numerical simulation gives rise to larger values of the force acting on the foil both during the negative phase of the manoeuvre

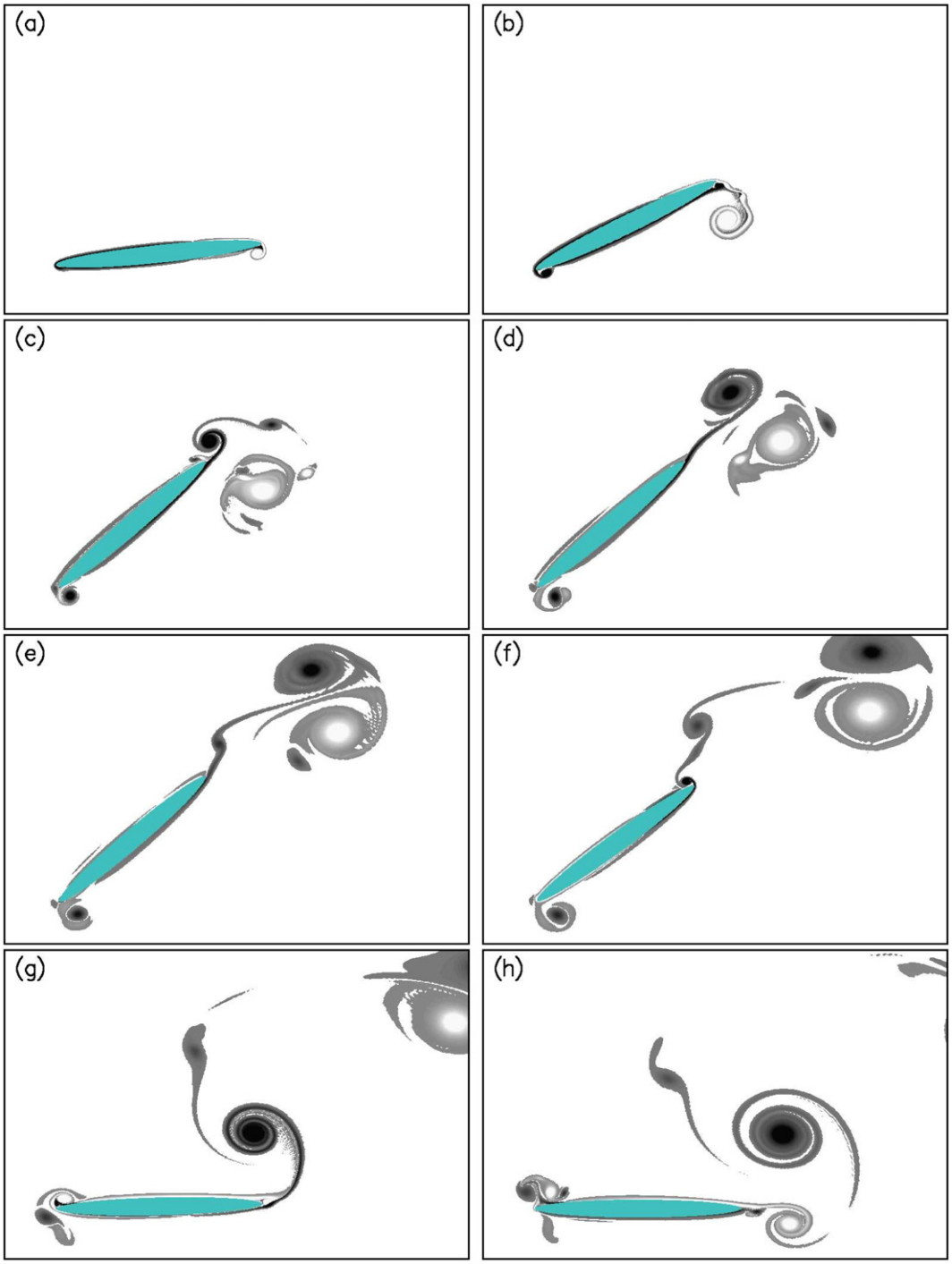

Fig. 5. Vorticity fields at $t^* = 0.272$ s, $t^* = 0.343$ s, $t^* = 0.486$ s, $t^* = 0.63$ s, $t^* = 0.873$ s, $t^* = 0.917$ s, $t^* = 1.06$ s, $t^* = 1.2$ s. The parameters are those of the experiment of [2].

and when the foil generates a positive thrust. Moreover, the peak of the negative precursor force in [1] occurs right after $t^* = T_r^*$, whereas it takes place before $t^* = T_r^*$ in Fig. 2. Similarly, the positive peak force in [1] occurs after $t^* = T^*$ whereas it is before $t^* = T$ in Fig. 2. Finally, after the first positive peak, significant fluctuations bring to vanishing values of the thrust, while the experimental measurements display a plateau at a non-zero thrust.

As already pointed out, the numerical 'experiments' allow the measurement and analysis of many other quantities. In Fig. 4 the transverse force F_y^* acting on the foil is plotted versus time along with the torque M_z^*. The results show that a sideways reaction force is present both during the upward rotation and the downward rotation, even though the average value almost vanishes. The evaluation of the force acting on the foil is made after the pressure p^* is computed from momentum equation. Then, the integration of the pressure and the viscous stresses on the foil surface provides the force components F_x^* and F_y^*. Because of this procedure, it is not possible to separate the different contributions to the force usually identified in the text books (e.g. drag force, added mass force,...). Fig. 5 shows the time development of the vortex structures shed by the foil. Just after the start of the upward rotation, a clockwise rotating vortex begins to develop at the moving edge

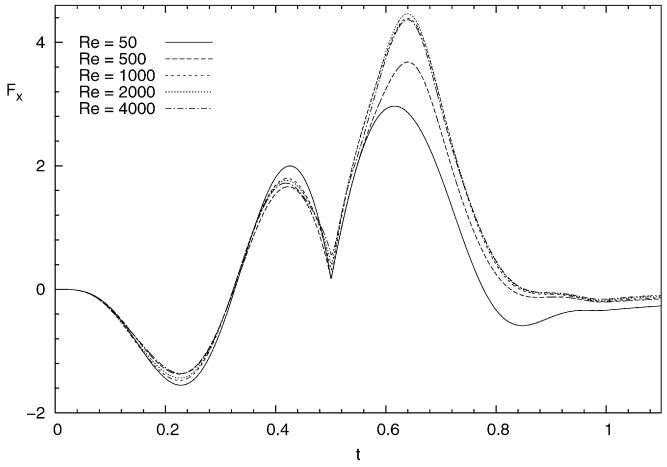

Fig. 6. Propulsive force F_x acting on the foil during a rotation defined by the kinematics (1), for different values of the Reynolds number. $T_e = 0$, $\alpha_{\max} = -30°$.

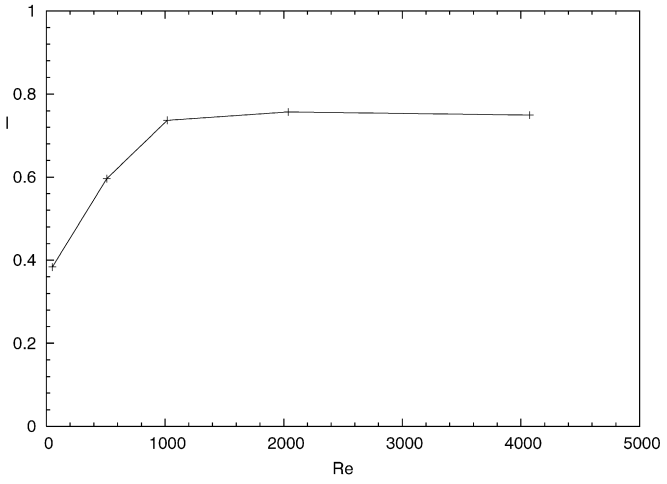

Fig. 7. Dimensionless impulse I acting on the foil for different values of the Reynolds number and $T_e = 0$, $\alpha_{\max} = -30°$.

of the foil (see Fig. 5(a)). Later on, further vorticity is shed by the edge of the foil and the size of the vortex increases. A Helmholtz instability of the free shear layer which leaves the foil can be observed (5(b)). Then the foil stops and the clockwise rotating vortex induces a flow field which causes flow separation from the edge of the foil and the formation of a counter-clockwise rotating vortex (5(c)). This vortex couples with the previous one and gives rise to a vortex pair which moves far from the foil because of the self induced velocity (5(d)). Simultaneously, a jet of fluid is created and a propulsive force appears. Then the vortices decay because of the viscous effects and the foil starts its downward rotation (5(e)). A counter-clockwise vortex is generated (5(f), (g)) which gives rise to a new clockwise vortex and a new vortex pair when the foil stops (5(h)). Small vortices are also shed by the opposite edge of the foil which does not move significantly, but they are very weak and do not give rise to any relevant force.

Notwithstanding the quantitative differences between the numerical results and the laboratory measurements previously discussed, the present model seems to capture the main features of the phenomenon and it can be fairly used to investigate how the parameters of the problem affect the results. Indeed, further comparisons between the numerical results and the laboratory data by [3], which are described in [11], support the reliability and accuracy of the numerical code.

4. Discussion of the results

If the problem is made dimensionless using the chord c^* of the foil as length scale, the duration $2T_r^*$ of the counter-clockwise and clockwise rotations as time scale and $c^*/2T_r^*$ as characteristic velocity of the phenomenon, a simple dimensional analysis shows that the propulsive force depends only on the maximum angle of rotation $\alpha_{\max}$ and on the Reynolds number Re defined as $Re = c^{*2}/(2\nu^* T_r^*)$ (ν^* is the kinematic viscosity of the fluid), beside the details of the kinematics of the foil. In practical applications, the values of the Reynolds number turn out to be large and viscous effects are confined within the thin boundary layers which are generated along the foil surface by the no-slip condition. Then, the vorticity is shed in the free stream because the boundary layers leave the foil, as free shear layers, at the edges of the foil where the external flow strongly decelerates. Eventually, the free shear layers give rise to large vortex structures whose dynamics is essentially inviscid. Therefore, the Reynolds number is expected to play only a minor role in the phenomenon. This fact is confirmed by the results shown in Fig. 6, where the dimensionless propulsive force per unit width $F_x = F_x^* \rho^* c^{*3}/(2T_r^*)^2$ is plotted versus time for the same kinematics of the foil, such that $T_e = 0$ and $\alpha_{\max} = -30°$, but for different values of the Reynolds number. Indeed, the values of F_x significantly change only when the Reynolds number is smaller than 1000, but they are practically constant for larger values. This finding is summarized in Fig. 7, where the dimensionless impulse per unit width $I = \int_0^T F_x(t)\,dt = \int_0^{T^*} F_x^*(t^*)\,dt^*/(\rho^* c^{*3}/2T_r^*)$ is plotted versus the Reynolds number.

The propulsive performance of a fast start can be evaluated by quantifying various distance-time parameters (for example, distance traveled within a given time, mean and maximum forward velocity, ...). In the present work, the propulsive force F_{Tx}^* induced by the foil motion is used to move a fish body which is supposed to be characterized by a given volume V^*, a section A^* and fixed values of the added mass c_M and drag c_D coefficients. Therefore, the propulsive force, which is opposed by drag and added mass forces, gives rise to the motion of the fish described by

$$\rho^*(1+c_M)V^*\frac{d^2x_m^*}{dt^{*2}} + \frac{1}{2}\rho^* A^* c_D \frac{dx_m^*}{dt^*}\left|\frac{dx_m^*}{dt^*}\right| = F_{Tx}^*, \tag{2}$$

where x_m^* is the displacement of the fish, the averaged density of which is supposed to be equal to that (ρ^*) of the water. The numerical integration of (2), performed simultaneously with the evaluation of the propulsive force $F_{Tx}^* = F_x^* S$ generated by the oscillating tail (whose span width S^* is presently assumed equal to $4c^*$), allows to compute the dynamics of the fish and in particular the useful work exploited by the foil W_u^* and the input work W_d^*. The former quantity is defined by $\int_0^{t^*} F_{Tx}^*(dx_m^*/d\tau^*)\,d\tau^*$ while the latter turns out to be $\int_0^{t^*} F_{Ty}^*(dh_0^*/d\tau^*)\,d\tau^* + \int_0^{t^*} M_{Tz}^*(d\alpha/d\tau^*)\tau^*$, where M_{Tz}^* is the torque acting on the foil.

Hence, it is possible to compute the efficiency $\eta = W_u^*/W_d^*$ of the manoeuvre along with other interesting quantities like the velocity of the fish. Ahlborn et al. [2] suggest that a stronger thrust is generated if a small time interval elapses between the counter-clockwise rotation and the clockwise one, i.e. if values of T_e^* different from zero are used. Therefore, a set of runs is made by fixing the maximum angle of rotation $\alpha_{\max}$ equal to $-30°$, the Reynolds number equal to 2000 and changing the value of $T_e = T_e^*/2T_r^*$. Moreover, having in mind a medium size fish, $(1+c_m)V^*/c^{*2}$ is set equal to 25 and $c_D A^*/(2c^*)$ equal to 5 even though different choices of these values do not induce qualitative changes in the obtained results. Fig. 8 shows the propulsive force F_x versus time for $0 \leqslant T_e \leqslant 0.5$. After the counter-clockwise rotation, a positive, almost constant, value of the propulsive force can be observed when the plate keeps its maximum rotation angle. The propulsive

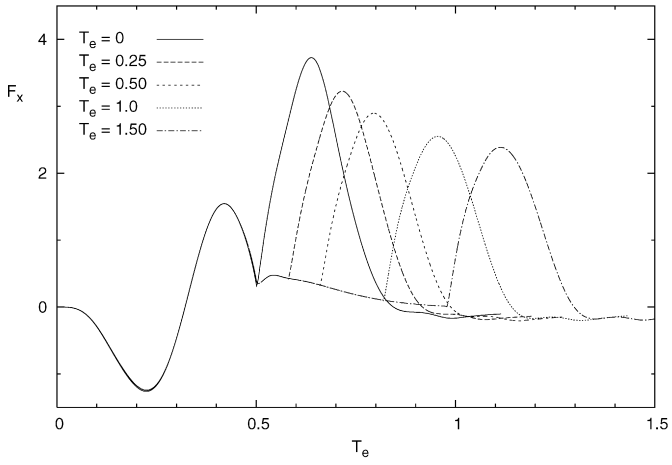

Fig. 8. Dimensionless force acting on the foil F_x. The foil motion is characterized by $Re \simeq 2000$ and the kinematics (1), where $\alpha_{\max} = -30°$ and T_e is varied between 0 and 0.5.

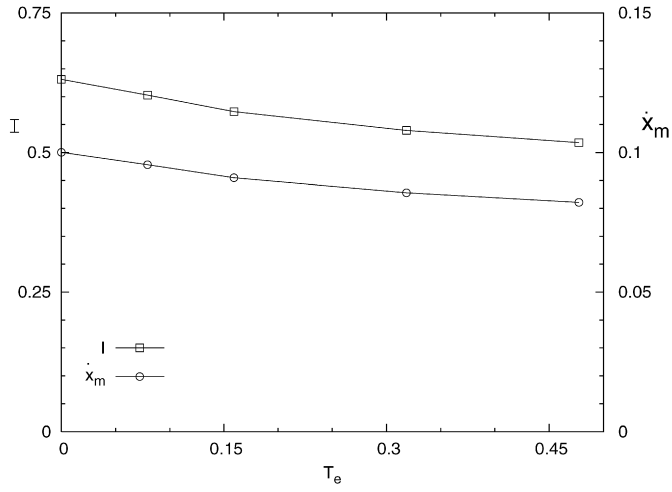

Fig. 9. Dimensionless impulse acting on the foil and final velocity of the body propelled by the foil. The foil motion is characterized by $Re \simeq 2000$ and the kinematics (1), where $\alpha_{\max} = -30°$ and T_e is varied between 0 and 0.5.

force is generated as a reaction to the jet of fluid created by a vortex pair similar to that which appears in Figs. 5(c), 5(d). The counter-clockwise rotating vortex becomes stronger during the foil stop because of the flow induced close to the trailing edge by the clockwise vortex generated during the upward rotation. However, the propulsive force peak during the clockwise rotation decreases when the value of T_e is increased. The results are summarized in Fig. 9, where the dimensionless impulse and the final velocity of the body propelled by the rotating foil are plotted versus T_e. The impulse and the final velocity increase as T_e is decreased. Therefore, it appears that there is no advantage to stop the foil motion for a short time interval between the counter-clockwise and clockwise rotations of the foil. Moreover, the dimensional analysis shows that the propulsive force and the final velocity achieved by the fish are inversely proportional to the duration $2T_r^*$ of the manoeuvre and hence it would be convenient to perform the manoeuvre in the shortest possible time. However, it is evident that the finite muscular power of the fish sets a limit to $2T_r^*$.

It is also of interest to investigate the phenomenon by fixing the kinematics of the foil and simulating different values of $\alpha_{\max}$. From a qualitative point of view, only minor changes are present when different values of $\alpha_{\max}$ are considered. Indeed, Fig. 10, where the propulsive force F_x is plotted versus time, shows that whatever

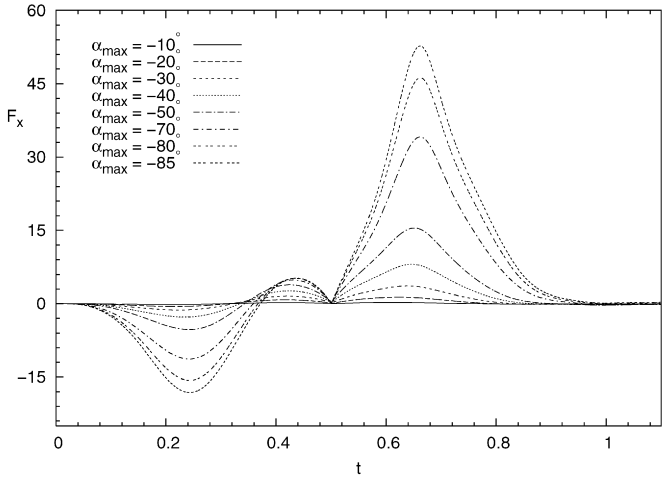

Fig. 10. Propulsive force F_x acting on the foil during its rotation, characterized by the kinematics (1), where $T_e = 0$ and $\alpha_{\max}$ is varied between $-10°$ and $-85°$.

value of $\alpha_{\max}$, there is an initial period during which a negative force F_x is generated which, after having attained it maximum value at about $t = 0.25$, decreases and reverses to become positive. During the clockwise rotation, the force is always positive. From a qualitative point of view, it is worth pointing out that the value of t, such that the force reverses its direction, slightly increases with increasing values of $\alpha_{\max}$. Since the numerical model can allow more complex manoeuvres of the fish tail, a further set of runs is made allowing both a heaving and a pitching motion, i.e. making more realistic simulations of the actual kinematics of a fish tail. In particular, to mimic the kinematics of a fish tail during both C and S starts, the following relations are used

$$h(t) = \begin{cases} 0 \\ g_1(t) \\ h_0 \sin \pi t \\ g_2(t) \\ 0 \end{cases}$$

$$\alpha(t) = \begin{cases} 0 & \text{for } t < 0 \\ f_1(t) & \text{for } 0 < t < T_r \\ \alpha_{\max} \sin(\pi t + \varphi) & \text{for } T_r < t < 1 - T_r \\ f_2(t) & \text{for } 1 - T_r < t < 1 \\ 0 & \text{for } t > 1 \end{cases} \tag{3}$$

in which the chord c^* of the foil is the length scale and the whole duration T^* of the manoeuvre is the time scale. The functions f_1, f_2, g_1, g_2 are fifth order polynomial functions such that α and h turn out to be continuous along with their first and second derivatives. The values of both h_0 and $\alpha_{\max}$ are inferred from the sketches drawn in Domenici and Blake [6]. Indeed, the oscillations of the peduncle of a fish tail give rise to a transverse motion of the whole tail. To give to the reader an idea of the tail kinematics, its position is shown in Fig. 11 in a fixed reference frame, superimposing the forward motion of the fish. As already discussed, since the Reynolds number assumes large values, the dynamics of the vortex structures shed by the foil is essentially inviscid. Moreover, because separation takes place at the leading and trailing edges of the foil and its location does not depend on the Reynolds number, the values of Re have no great influence on the results, which are affected by the amplitudes $\alpha_{\max}$ and h_0 of the angular and transverse oscillations, by the phase angle φ and by the value of T_r. The minor role of the Reynolds number in the phenomenon is confirmed by the results shown in Fig. 12, where the impulse I and the final velocity $\dot{x}_m$ of the fish body are plotted versus Re, where $Re = c^{*2}/(\nu^* T^*)$. Indeed, the values of both I and $\dot{x}_m$ do not show any appreciable variation when different values of the Reynolds number are considered.

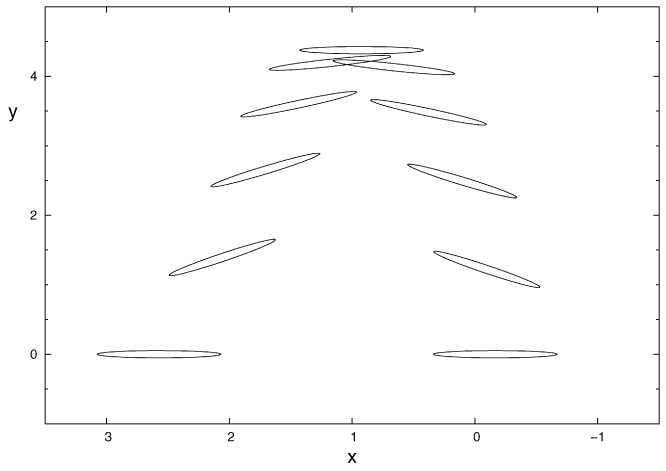

Fig. 11. Position of the foil during a fast start manoeuvre characterized by the kinematics (3), taking into account the induced forwards motion of the fish. The elapsed time between successive positions is one tenth of the whole duration of the manoeuvre. The body moves from right to left.

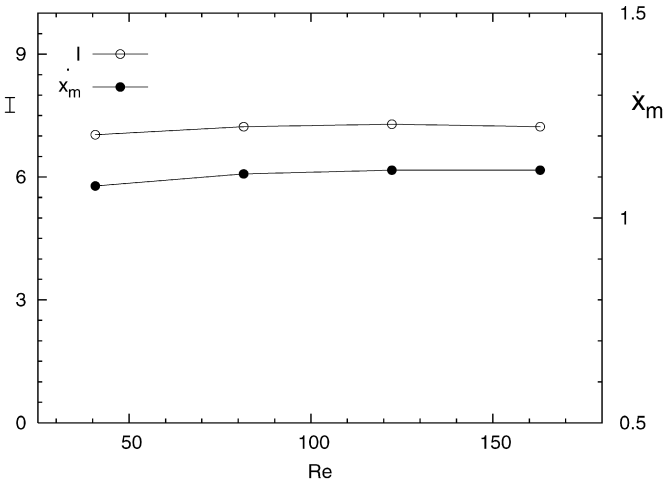

Fig. 12. Dimensionless impulse I associated to the propulsive force F_x acting on the foil and final velocity $\dot{x}_m$ of the body propelled by the foil for various values of the Reynolds number. The foil motion is characterized by the kinematics (3) with $\alpha_{max} = 35°$, $h_0 = 1.25$, $\varphi = 90°$ and $T_r = 0.127$.

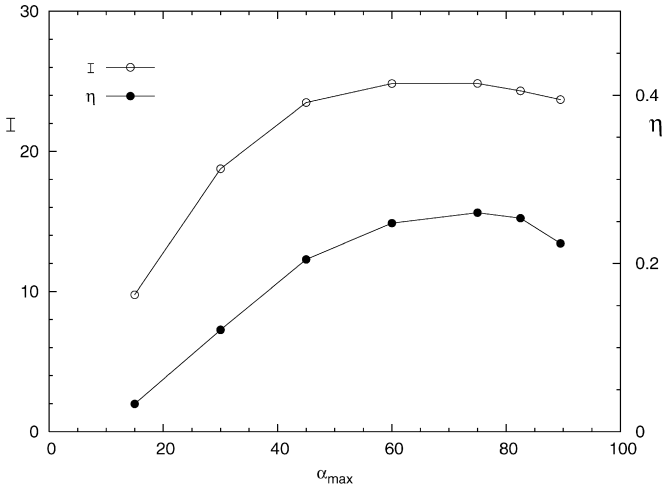

Fig. 13. Dimensionless impulse I acting on the foil and efficiency η_P for different values of the amplitude α_{max} of the angular oscillations. The foil motion is characterized by the kinematics (3) with $Re = 20.4$, $h_0 = 2.5$, $\varphi = 90°$ and $T_r = 0.127$.

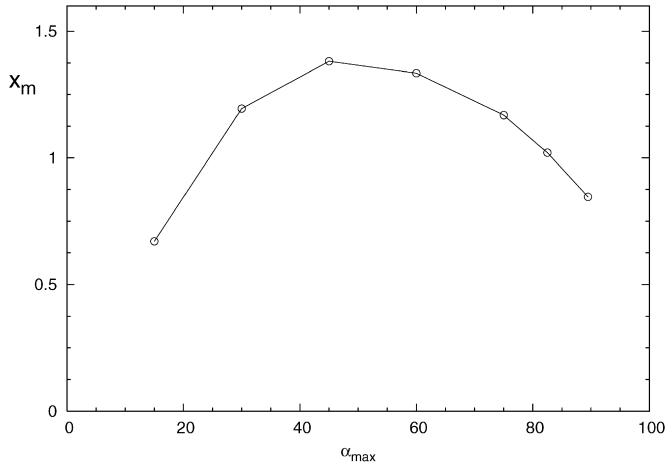

Fig. 14. Final dimensionless displacement x_m of the body propelled by the foil for different values of the amplitude α_{max} of the angular oscillation. The foil motion is characterized by the kinematics (3) with $Re = 20.4$, $h_0 = 2.5$, $\varphi = 90°$ and $T_r = 0.127$.

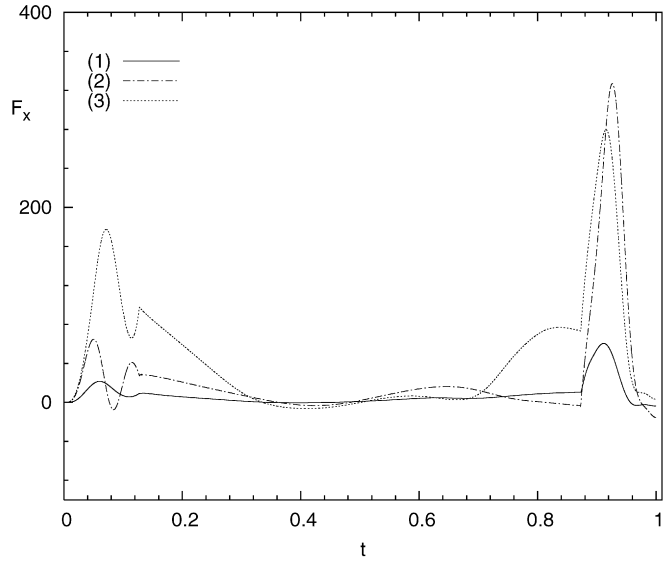

Fig. 15. Dimensionless propulsive force F_x acting on the foil which moves accordingly to the kinematics (3), for three cases: (1) $Re = 163$, $\alpha_{max} = 35°$, $h_0 = 1.25$, $\varphi = 90°$, $T_r = 0.127$; (2) $Re = 20.4$, $\alpha_{max} = 75°$, $h_0 = 2.5$, $\varphi = 90°$, $T_r = 0.127$; (3) $Re = 11.6$, $\alpha_{max} = 35°$, $h_0 = 4.375$, $\varphi = 90°$, $T_r = 0.127$.

Fig. 13 shows the impulse and the efficiency as function of the angle α_{max}. The results suggest that during a fast start, the kinematics of which is described by (2), the tail of a fish provides the maximum thrust and the maximum efficiency when the maximum rotation angle ranges between 60° and 80°, which are values in some cases displayed by the sketches of [6], who analyzed the strike pattern in a pike and in an angelfish. As already pointed out, the propulsive performances of a fast start can be evaluated by quantifying various distance-time parameters. If the distance traveled by the body is considered (see Fig. 14) the optimal manoeuvre is that characterized by a value of α_{max} close to 45°. Hence, the goal of the manoeuvre (maximum impulse, maximum final velocity, maximum distance) should be carefully selected.

It is interesting to analyze the time development of the propulsive force, per unit width of the foil, which is shown in Fig. 15 for some of the numerical simulations. Indeed, the rotation of the foil coupled with its transverse motion makes the negative precursor disappear and the x-component of the force turns out to be positive during almost the whole manoeuvre. An example of the

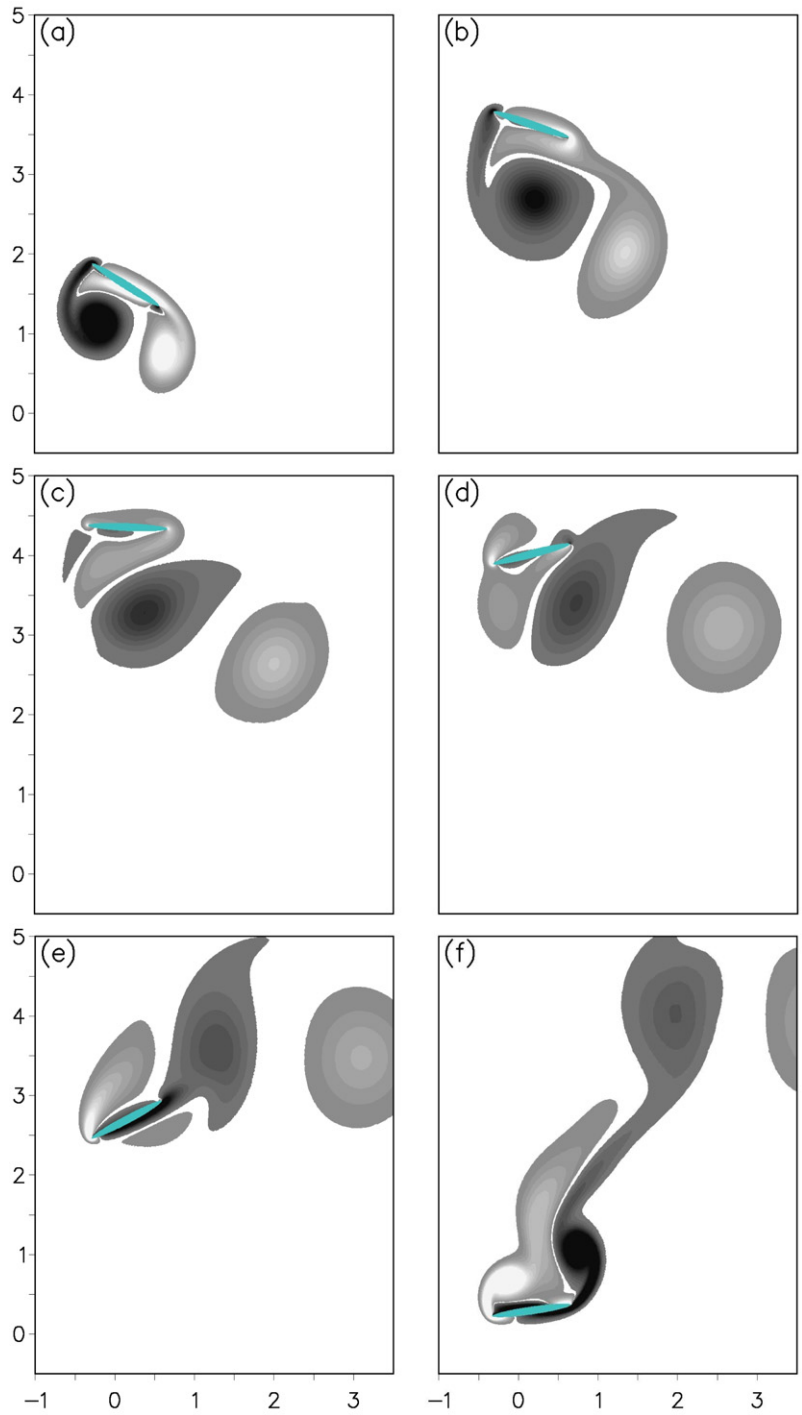

Fig. 16. Vorticity fields at $t = 0.127$, $t = 0.318$, $t = 0.48$, $t = 0.64$, $t = 0.8$, $t = 0.95$, for $Re = 11.6$, $\alpha_{max} = 35°$, $h_0 = 4.375$, $\varphi = 90°$, $T_r = 0.127$ (case 3 of Fig. 15)

vorticity fields during the manoeuvre of the heaving and pitching foil is displayed in Fig. 16. Comparing Fig. 16 with Fig. 5, where the vorticity fields are displayed for a foil which rotates only, the main difference is due to the large vortex structure shed by the leading edge, which are absent in the results for the rotating foil. Moreover, Fig. 16 shows that the counter-clockwise rotating vortex shed by the leading edge subsequently merges with the positive vorticity shed by the trailing edge thus originating a unique counter-clockwise vortex structure. In the meanwhile, the clockwise rotating vortex generated by the trailing edge from the beginning of the foil motion moves away from the foil and further negative vorticity is shed by the leading edge during the downward motion of the foil. Fig. 17 shows the pressure distribution along the foil surface during the first part of the manoeuvre for both the cases considered in Figs. 5 and 16. When the foil rotates only, the negative force which appears at the beginning of the manoeuvre is due to the larger values of the pressure distribution along the upper part of the foil with respect to those appearing along the lower part of the foil (the reader should note that the angle θ is zero at the trailing edge and it is positive in the counter-clock wise direction) and to the negative angle of the foil with respect to the required direction of motion. Then the pressure difference between the upper and lower surfaces of the foil decreases and this leads to a decrease of the resistance force. A similar pressure distribution is

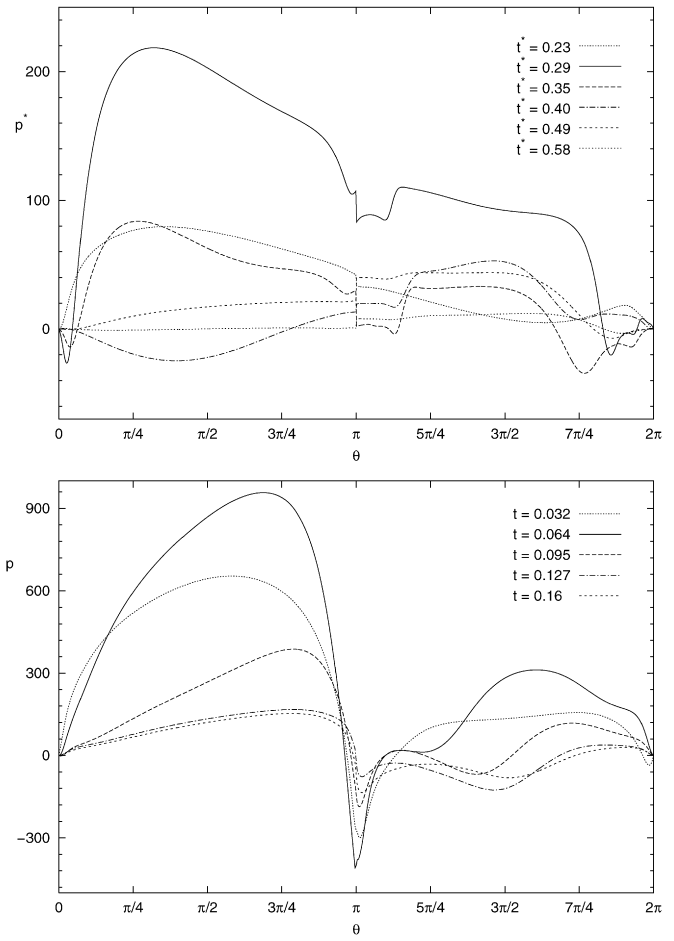

Fig. 17. Pressure distribution along the foil surface during its rotation up to the maximum angle. In the top figure the dimensional pressure is plotted when the parameters are those of the experiment of [2], like in Figs. 2–5; in the bottom figure the dimensionless pressure is plotted for $Re = 11.6$, $\alpha_{max} = 35°$, $h_0 = 4.375$, $\varphi = 90°$, $T_r = 0.127$ (case 3 of Fig. 15).

found for the heaving and pitching foil but the positive rotation of the foil gives rise to a propulsive force. In the top panel of Fig. 17, t^* is the dimensional time which appears also in Fig. 2. Hence $t^* = 0.23$ s is just after the start of the manoeuvre and $t^* = 0.58$ s is during the foil stop at the maximum angle. In the lower panel of Fig. 17, the dimensionless time is given which also appears in Fig. 15.

The identification of the optimal value of h_0 is not simple. Indeed, even though the efficiency of the manoeuvre displays a relative maximum as h_0 is increased, the impulse and the final velocity monotonically increase when h_0 are increased (see Fig. 18). Similarly the impulse and the fish velocity increase monotonically as T_r is decreased (see Fig. 19). The need of a rapid start to escape from a predator or to perform a rapid attack to get the food for survival suggests a manoeuvre characterized by a high value of h_0 and a very short time T_r. However, geometrical constraints and the large peaks of the force which is necessary to generate the tail movements limit the values of h_0 and T_r.

5. Conclusions

The flow field generated by an aperiodic rigid body motion of a foil is investigated by means of numerical experiments. The investigation is carried out to gain information on the efficiency of a flapping foil to manoeuvre underwater vehicles.

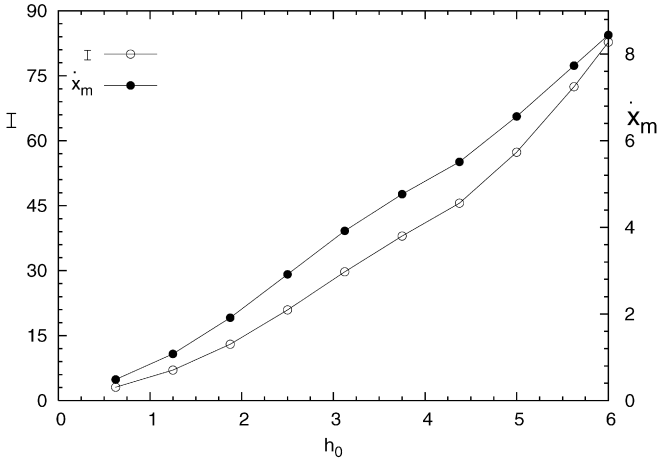

Fig. 18. Dimensionless impulse I and final velocity $\dot{x}_m$ of the body propelled by the foil for various values of the amplitude h_0 of the transverse oscillations. The foil motion is characterized by the kinematics (3) with $\alpha_{max} = 35°$, $\varphi = 90°$ and $T_r = 0.127$. The Reynolds number Re is inversely proportional to h_0.

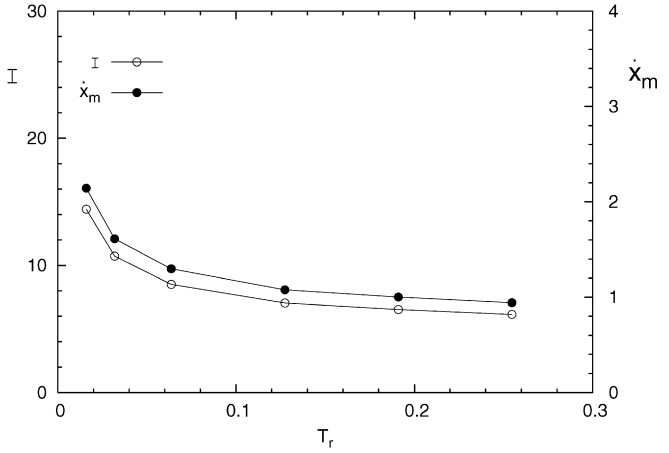

Fig. 19. Dimensionless impulse I associated to the propulsive force F_x acting on the foil and final velocity $\dot{x}_m$ of the body propelled by the foil for various values of the time T_r, during which the foil reaches the maximum angle of rotation. The foil motion is characterized by the kinematics (3) with $Re = 40.7$, $\alpha_{max} = 35°$, $\varphi = 90°$ and $h_0 = 1.27$.

The numerical approach, which was previously supported by a comparison between its predictions and the experimental measurements of [3], is further tested by comparing the computed force with the data obtained by [2], who measured the propulsive force generated by a rotating plate which simulates the tail of a fish performing a fast start. Then, numerical simulations are made both for a foil which rotates around its leading edge and for a pitching and heaving foil. The obtained results show that some characteristics of the kinematics of the foil can be chosen to maximize the propulsive force. However, the force monotonically increases when the amplitude of the lateral motion of the foil is increased and the duration of the manoeuvre is decreased.

Even though the rigid body motion of the foil is chosen to mimic a fish tail during a fast start, the foil should be considered only as a first order approximation of a fish tail, which is observed to deform in real life. Therefore, the investigation helps to understand the basic mechanism through which fish achieve high acceleration during fast starts, but quantitative differences are expected to be present between the computed flow and the actual one, which is also significantly affected by the finite span of fish tails.

Acknowledgements

Thanks are due to the office of Naval Research under contract No. 000140310193 monitored by Dr. Thomas F. Swean.

References

[1] B. Ahlborn, S. Chapman, R. Stafford, R.W. Blake, D. Harper, Experimental simulation of the thrust phases of fast-start swimming of fish, Journal of Experimental Biology 200 (1997) 2301–2312.
[2] B. Ahlborn, D.G. Harper, R.W. Blake, D. Ahlborn, M. Cam, Fish without footprints, Journal of Theoretical Biology 148 (1991) 521–533.
[3] J.M. Anderson, K. Streitlien, D.S. Barret, M.S. Triantafyllou, Oscillating foils of high propulsive efficiency, Journal of Fluid Mechanics 360 (1998) 41–72.
[4] P. Blondeaux, F. Fornarelli, L. Guglielmini, M.S. Triantafyllou, R. Verzicco, Numerical experiments on flapping foils mimicking fish-like locomotion, Physics of Fluids 17 (11) (November 2005).
[5] P. Domenici, R.W. Blake, The kinematics and performance of the escape response in the angelfish (*pterophyllum eimekei*), Journal of Experimental Biology 156 (1991) 187–205.
[6] P. Domenici, R.W. Blake, The kinematics and performance of fish fast-start swimming, Journal of Experimental Biology 200 (1997) 1165–1178.
[7] H. Dong, R. Mittal, F.M. Najjar, Wake topology and hydrodynamic performance of low-aspect-ratio flapping airfoil, Journal of Fluid Mechanics 566 (2006) 309–343.
[8] C.P. Ellington, The aerodynamics of hovering insect flight – IV aerodynamic mechanism, Philosophical Transactions of the Royal Society of London, Series B 305 (1984) 79–113.
[9] P. Freymuth, Visualizing the connectivity of vortex systems for pitching wings, Journal of Fluids Engineering 111 (1989) 217–220.
[10] L. Guglielmini, Modeling of thrust generating foil, PhD thesis, Environmental Engineering Department, University of Genoa, May 2004.
[11] L. Guglielmini, P. Blondeaux, Propulsive efficiency of oscillating foils, European Journal of Mechanics B/Fluids 23 (2) (2004) 255–278.
[12] G.C. Lewin, H. Haj-Hariri, Modelling thrust generation of a two-dimensional heaving airfoil in a viscous flow, Journal of Fluid Mechanics 492 (2003) 339–362.
[13] K. Parker, K.D. von Ellenrieder, J. Soria, Using stereo multigrid *dpiv* (*smdpiv*) measurements to investigate the vortical skeleton behind a finite-span flapping wing, Experiments in Fluids 39 (2) (August 2005).
[14] G. Pedro, A. Suleman, N. Djilali, A numerical study of the propulsive efficiency of a flapping hydrofoil, International Journal for Numerical Methods in Fluids 42 (2003) 493–526.
[15] Z.J. Wang, Vortex shedding and frequency selection in flapping flight, Journal of Fluid Mechanics 410 (2000) 323–341.
[16] P.W. Webb, J.M. Skadsen, Strike tactics of Esox, Canadian Journal of Zoology 58 (1980) 1462–1469.